

# Studies on surface treatment of electrodeposited Ni–Zn alloy coatings using saccharin additive

A . C. Lokhande<sup>1</sup> · A. Shelke<sup>2</sup> · P. T. Babar<sup>1</sup> · J. S. Bagi<sup>3</sup> · Jin Hyeok Kim<sup>1</sup>

Received: 16 September 2016 / Revised: 8 March 2017 / Accepted: 10 March 2017 / Published online: 29 March 2017  
© Springer-Verlag Berlin Heidelberg 2017

**Abstract** Ni–Zn alloy coatings were electrodeposited galvanostatically at room temperature. Saccharin (0 to 1.8 g L<sup>-1</sup>) was added in the deposition bath as an additive agent. The effects of varied saccharin content addition on the physical properties of Ni–Zn alloy coatings were studied. The Ni–Zn alloy coatings were characterized using X-ray diffraction (XRD), scanning electron microscopy (SEM), atomic absorption spectroscopy (AAS), atomic force microscopy (AFM), contact angle, electrochemical impedance study (EIS), salt immersion test, friction coefficient, and wear resistance tribology techniques. The XRD study confirmed the formation of Ni–Zn alloys with mixed phases of Ni–Zn alloy depending upon the saccharin content addition. The AAS analyses based on varied saccharin addition confirmed Ni–Zn alloy composition between 64:36 and 22:78 at.%. The effects of varied saccharin addition on physical properties like stress, strain, microstructure, topography, wettability, wear, and corrosion resistance were studied. The optimized 1.6 g L<sup>-1</sup> saccharin addition in the deposition bath with Ni–Zn composition as 25:75 at.% possesses highly enhanced surface

properties like compact, smooth microstructure, and increased corrosion resistance with reduced friction coefficient value.

**Keywords** Electrodeposition · Ni–Zn alloy · Friction coefficient · Corrosion resistance

## Introduction

For many years, zinc and cadmium coatings have been used for corrosion protection application. Cadmium coatings are produced from toxic cyanide bath, and they produce carcinogenic effects, hence their use is restricted [1], whereas zinc-based zinc–nickel–cadmium alloy coating produces toxic hexavalent compounds [2]. Due to development in coating technology, toxic cadmium and zinc coatings are replaced with Zn and Ni alloy coatings such as Zn–Ni and Ni–Co alloys as they exhibit overall good performance [3]. Materials in the nanoscale show enhanced chemical and mechanical properties. The alloy coatings in the grain size range of 20–100 nm exhibit improved mechanical properties [4]. Electrodeposition technique produces nanosized grains and has advantages such as low cost and high production rate [5]. The alloys have been deposited from both simple and complex bath. Deposition from sulfate bath produces low stressed deposits [6].

Electrodeposition of Zn–Ni alloys has acquired great attention due to their application in various fields such as oil, gas, aerospace, automobiles, and electronics. Many studies have reported deposition of Zn–Ni alloy as anomalous, wherein less noble metal (Zn) is preferentially deposited. Still, a detailed study regarding the deposition type of Zn–Ni alloy is not fully revealed [7–9]. Rao et al. [7] reported that experimental parameters such as temperature, pH, polarization, and bath composition are responsible for producing normal and anomalous deposition of Zn–Ni alloys. The majority of the work is

✉ J. S. Bagi  
jaysbagi@gmail.com

✉ Jin Hyeok Kim  
jinhyeok@chonnam.ac.kr

A . C. Lokhande  
abhi4502@gmail.com

<sup>1</sup> Optoelectronic Convergence Research Centre, Department of Materials Science and Engineering, Chonnam National University, Gwangju 500-757, South Korea

<sup>2</sup> Thin Film Physics Laboratory, Department of Physics, Shivaji University, Kolhapur, MS 416 004, India

<sup>3</sup> Department of Technology, Shivaji University, Kolhapur, Maharashtra, India

reported on the electrodeposition and characterization of Zn–Ni alloy coating and their properties like corrosion resistance, friction coefficient, and surface morphology. The effects of direct current and peak pulse current on the deposition of Zn–Ni alloy have been studied by Sorkhabi et al. [10]. Effects of temperature on the deposition of Zn–Ni alloy coatings have been reported by Qiao et al. [11].

Electrodeposition of ternary alloys such as Zn–Ni–Fe and Zn–Ni–Co and their mechanical properties have been studied [12, 13]. Several additive agents like saccharin, naphthalene, and trisulphonic acid are used during a deposition for enhancing the mechanical properties of the alloy coatings. Mosavat et al. [3] reported that electrodeposition of Zn–Ni alloy from glycine bath using saccharin as an additive resulted in the reduced crystallite size and surface roughness value of the alloy coatings. Saccharin addition plays an important role in the deposition of the Ni-based alloy coatings such as producing smooth, low stressed, and compact deposits. Li et al. [5] studied the effect of saccharin content on the microhardness of Ni–Co alloy stating that the microhardness depends upon the content of saccharin addition which induces grain refinement.

The present investigation reports the electrodeposition of Ni–Zn alloy coatings using a varied amount of saccharin as an additive agent. The effects of the varied amount of saccharin addition on the physical properties of Ni–Zn alloy coatings such as composition, corrosion resistance, surface morphology, structure, stress, strain, wettability, friction coefficient, and wear resistance are reported. The optimized 1.6 g L<sup>-1</sup> saccharin addition in the deposition bath with Ni–Zn composition as 75:25 at.% is suggested to achieve above desirable physical properties.

## Experimental details

Ni–Zn alloy coatings were electrodeposited at room temperature from an aqueous bath consisting nickel sulfate (250 g L<sup>-1</sup>) and zinc sulfate (40 g L<sup>-1</sup>). Sodium sulfate (30 g L<sup>-1</sup>) was used as an electrolyte for increasing the conductivity of the bath during deposition. Boric acid (35 g L<sup>-1</sup>) was used as a buffer to maintain pH, Triton X-100 (0.08 g L<sup>-1</sup>) as an anti-pitting agent, and saccharin (0–1.8 g L<sup>-1</sup>) as an additive agent was used. The pH of the solution was adjusted to 3.5 ± 0.1 using nickel carbonate and sulfuric acid. All solutions were prepared using double distilled water. The above preparative parameters were fixed by making various trial and errors. The electrodeposition was carried out on medium carbon steel (1 × 5 cm<sup>2</sup> area) strip substrates. The substrates were polished with sand paper followed by ultrasonic cleaning in distilled water. After that, the substrates were activated for 10 s in the 10 vol.% HCl solution followed by final rinsing in distilled water. A three-electrode system consisting of medium carbon steel substrate as a cathode, graphite as an anode, and saturated calomel electrode (SCE) as a reference electrode was used. Electrodeposition was carried out galvanostatically at a

current density of 5 mA cm<sup>-2</sup> using a Wonatech battery cyler potentiostat. The plating parameters like current density, electrolyte composition, and temperature were kept fixed, and only the concentration of the additive agent, saccharin, was varied from 0 to 1.8 g L<sup>-1</sup>. The Ni–Zn alloy coatings electrodeposited for 15 min resulted in the thickness of 5–7 μm.

Many by-products of the reaction may be formed upon cathodic reaction of saccharin due to the interaction of different chemical bonds and functional groups. The primary reactions are the formation of main by-products such as bezamide, benzylsultame, and o-toluene sulfonamide. The secondary reactions may involve the incorporation of sulfur and carbon. Even though these reactions happen at the cathode, the by-products are present only in the electrolyte. The reductions of these by-products happen well below the deposition potential of the Ni–Zn film at a constant current density of 5 mA cm<sup>-2</sup>.

The structural characterization and the stress induced in the electrodeposited Ni–Zn alloy films were carried out by analyzing X-ray diffraction (XRD) patterns obtained with *Cu K<sub>α</sub>* (λ = 1.5418 Å) radiation from a D2 PHASER model (Bruker AXS Analytical Instruments Pvt. Ltd.) in the span of angle 2θ between 10° and 90°. Surface morphology of the Ni–Zn alloy films was studied with a scanning electron microscope (SEM) (JEOL, JSM 6360). The elemental composition of the alloy coatings was estimated with an atomic absorption spectrophotometer (AAS) (Perkin Elmer Analyst 300). The surface wettability studies of the coating were carried out using a contact angle meter (Ramehart USA equipment) with a CCD camera. The topographic images were recorded with a multimode atomic force microscope (AFM) (Innova 1B3BE) operated in the contact mode. Corrosion resistance was studied with an electrochemical impedance spectrometer workstation (WonATech, zive SP5) and also with salt immersion test in 5% NaCl solution. The friction coefficient (μ) and the wear resistance were determined with an applied load of 6 N at 200 rpm on a pin on a disc tribometer (Ducom Instruments, India).

## Results and discussion

### Linear sweep voltammetry study of NiZn

In order to determine the deposition potential of Ni, Zn, and NiZn and evaluate the effect of saccharin addition in the bath on their deposition potential, linear sweep voltammetry (LSV) studies have been carried out on stainless steel substrates in the range –0.4 to –2 V vs SCE at a scan rate of 10 mV/s. Figure 1a–c shows LSV curves of Ni, Zn, and NiZn coatings at varied saccharin additions. The extrapolation of the curves gives the deposition potential as shown in Table 1. The deposition potential of Ni, Zn, and NiZn without saccharin addition in the bath is found

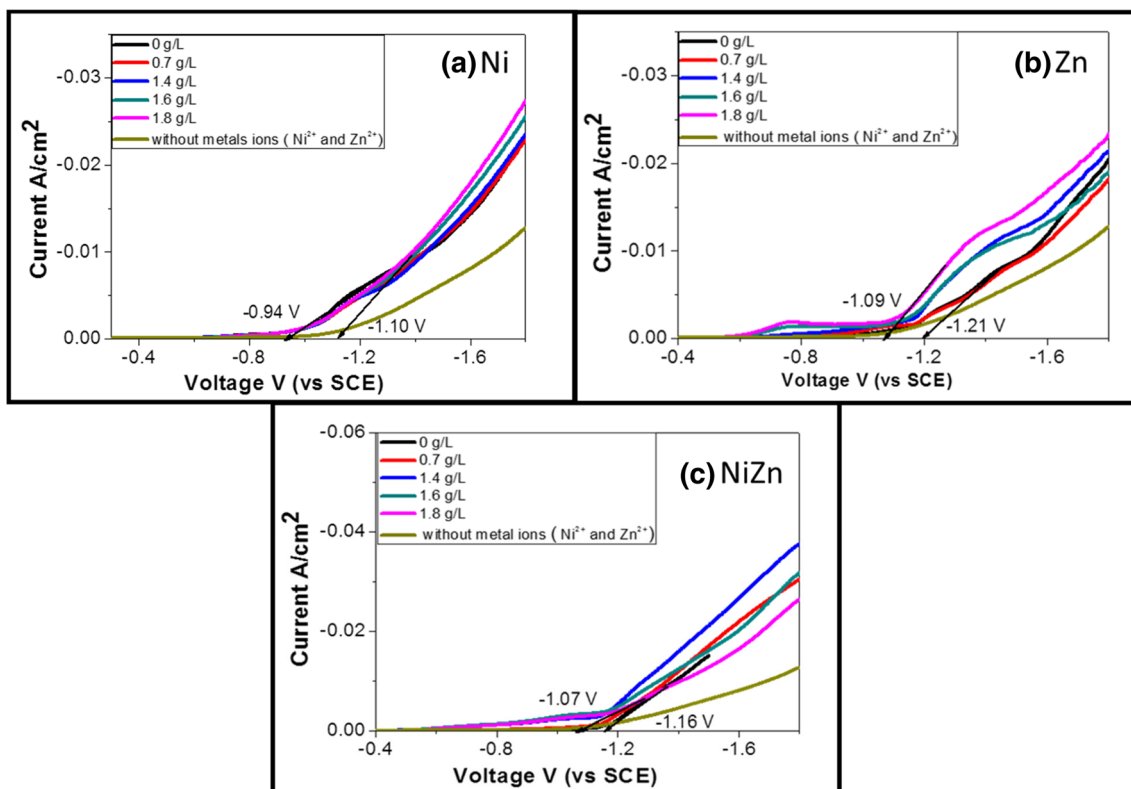


**Fig. 1** The linear sweep voltammetry (LSV) curves with varied saccharin content from 0 to 1.8 g L<sup>-1</sup> in the deposition bath of **a** Ni, **b** Zn, and **c** NiZn

to be -0.94, -1.21, and -1.16 V/SCE, respectively. The standard deposition potential of Ni and Zn is -0.57 and -0.99 V/SCE, respectively, with a potential difference of 0.42 V. The obtained deposition potentials for Ni and Zn in the study deviate from the standard deposition potential which can be attributed to the type of substrate (highly conducting) used, counter electrode, distance between two electrodes, conductivity of electrolyte, pH, and temperature [14]. As saccharin is added in the deposition bath, the deposition potential of Ni is increased (-0.94 to -1.10 V/SCE) and the deposition potential of Zn is reduced (-1.21 to -1.09 V/SCE), and hence, their corresponding potential difference decreases (0.27 to 0.01 V) which favors NiZn

alloy deposition. Hence, the reduction in the potential difference between the two metals (Ni and Zn) leads to alloy deposition.

The cathodic peak of the Zn deposition (Fig. 1b) is a combined effect of hydrogen evolution reaction peak and overpotential by water reduction. The observed peaks are attributed to the zinc-soluble products: zincate ion ((Zn(OH)<sub>4</sub>)<sup>2-</sup>) and soluble Zn<sup>2+</sup> species. Similarly, a Ni deposition cathodic peak (Fig. 1a) is also associated with hydrogen evolution peak. Hence, this induces a waviness nature in the LSV curves. As observed from the LSV curves of NiZn (Fig. 1c), each curve has two plateaus. The first plateau is attributed to Ni deposition limiting current, and the second plateau is attributed to the kinetically controlled Zn deposition. The obtained nature of the LSV curves for NiZn is different than the LSV curve obtained for Ni and Zn indicating the deposition of both metals (Ni and Zn) [14].

**Table 1** The calculated deposition potential of Ni, Zn, and NiZn using linear sweep voltammetry study (LSV)

Saccharin (g L <sup>-1</sup> )	Ni potential (V/SCE)	Zn potential (V/SCE)	Potential difference (V) between Ni and Zn	NiZn potential (V/SCE)
0	-0.94	-1.21	0.27	-1.16
0.7	-0.99	-1.19	0.20	-1.12
1.4	-1.03	-1.14	0.11	-1.10
1.6	-1.08	-1.11	0.03	-1.09
1.6	-1.10	-1.09	0.01	-1.07

**Composition of Ni–Zn alloy coatings**

The atomic percentage of the nickel and zinc in Ni–Zn alloy deposits was determined by AAS. The AAS study was carried out on alloys obtained by varying the amount of saccharin as 0, 0.7, 1.4, 1.6, and 1.8 g L<sup>-1</sup>. The AAS results confirmed the composition of Ni–Zn alloy between 64:36 and 22:78 at.%, as shown in Table 2. The analysis depicts that saccharin addition in the electrolyte bath produces an appreciable effect on the

**Table 2** The effect of saccharin content on the composition, crystallite size, residual stress, and lattice strain of Ni–Zn alloy coatings

Saccharin content (g L <sup>-1</sup> ) in deposition bath	Ni–Zn composition in at. %	Crystallite size (nm)	Compressive stress induced (MPa)	Lattice strain
0	64:36	25	-450	1.94
0.7	60:40	21	-410	1.73
1.4	30:70	18	-370	1.34
1.6	25:75	17.5	-310	0.85
1.8	22:78	23.5	-340	1.1

deposition of the alloy composition. Saccharin addition restricts the deposition of nickel in the Ni–Zn coating. Several reports indicate that in the case of Ni–Co alloy coatings, saccharin addition in the deposition bath hinders the deposition of cobalt and favors the deposition of nickel [5]. Also, the Zn content in the deposit is higher than that in the electrolyte bath indicating anomalous co-deposition of Ni–Zn alloy [11, 14–17]. According to electrochemical theory, due to the difference in the electropotential of nickel and zinc, nickel deposition must be prior to zinc deposition in the co-deposition of Ni–Zn alloy. However, the above mechanism is contradictory as in actual practice; zinc is preferentially deposited to nickel according to the suggested “hydroxide suppression mechanism” (HSM) [14]. As per HSM, hydrogen evolution during Zn deposition raises the pH at the cathode surface leading to the formation of Zn(OH)<sub>2</sub> which favors Zn deposition and restricts Ni deposition. Based on this mechanism, any parameter which can raise

the pH would favor preferential Zn deposition. When saccharin is used in an electrolyte bath, it is adsorbed on the cathode surface making it a hydrophobic surface which restricts H<sub>2</sub>O reduction near its vicinity eventually raising the pH at the cathode surface [15]. The increase forms a Zn(OH)<sub>2</sub> layer which restricts the flow of Ni ions from the electrolyte solution to the cathode surface. Hence, by varying saccharin contents in the electrolyte solution, pH correspondingly varies and hence the composition of Ni–Zn is varied.

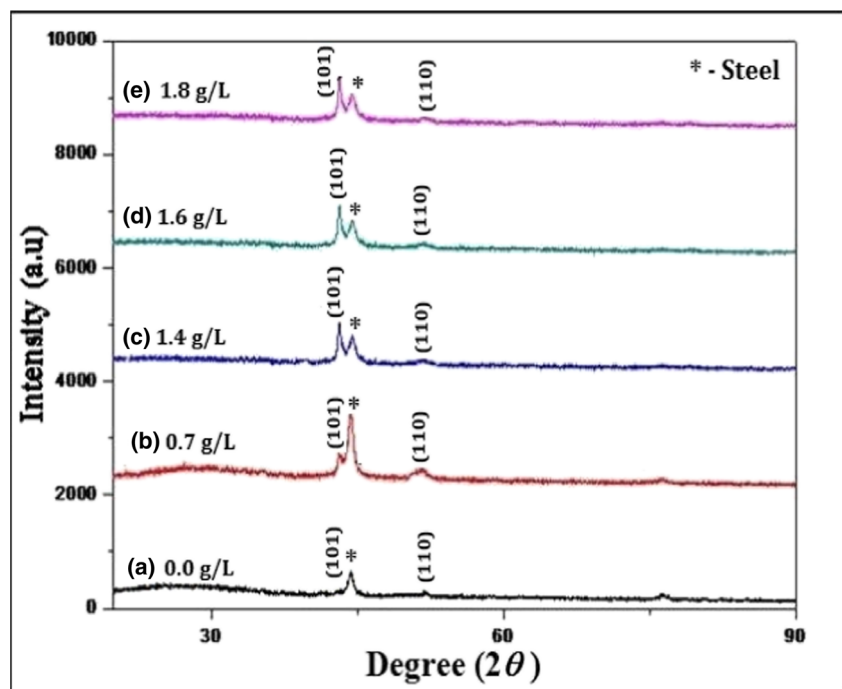
### Crystal structure and induced stress in Ni–Zn alloy coatings

Figure 2 (a–e) shows XRD patterns of the Ni–Zn alloy deposit with varied contents of saccharin addition (0–1.8 g L<sup>-1</sup>). The peaks marked by an asterisk are reflected from the steel substrate used for deposition. From Fig. 1, it is observed that the alloy of Ni–Zn is formed with major orientation along the (101) plane with an I4/mmm space group of tetragonal crystal structure and matches with JCPDS card No. 00-006-0672. The intensity of this peak increases as a content of saccharin into the Ni–Zn alloy up to 1.6 g/L due to the reduced strain. Reduced strain and enhanced (101) reflection at this composition indicate the formation of a crystalline tetragonal Ni–Zn alloy. The crystallite size of the Ni–Zn alloy was calculated using Scherer’s formula as

$$D = \frac{0.9\lambda}{\beta \cos\theta} \quad (1)$$

where  $\beta$  is the broadening of the diffraction line measured at half maximum intensity (radians),  $\lambda = 1.5404 \text{ \AA}$  is the

**Fig. 2** The XRD pattern of electrodeposited Ni–Zn alloy coating with varied saccharin content from a 0 g L<sup>-1</sup>, b 0.7 g L<sup>-1</sup>, c 1.4 g L<sup>-1</sup>, d 1.6 g L<sup>-1</sup> and e 1.8 g L<sup>-1</sup> on medium carbon steel substrate



wavelength of the  $Cu K_{\alpha}$  X-ray,  $D$  is the crystal size, and  $\theta$  is Bragg's angle. The deposited alloy consists of nanocrystals of about 17.5 nm for  $1.6 \text{ g L}^{-1}$ . It is reported earlier that saccharin raises the absolute cathodic overpotential. The nucleation rate is increased to produce nanosized grains [3]. Table 2 shows the crystallite size of the Ni–Zn alloy coating at different saccharin content additions. Residual stresses are induced in the deposit during electrodeposition. The induced stress may affect the physical, mechanical, and protective properties of the electrodeposits. High tensile stressed coatings are subjected to cracking, and hence, the stress induced must be low as possible. Low compressive stress is desirable as it helps to maintain the adhesive bond between the coating and the substrate [17]. The stress induced in the electrodeposited Ni–Zn alloy coatings along with lattice strains is determined from the XRD study using the “H Digital” software. The microstrains were calculated using the formula presented below in Eq. 2.

$$\beta = [\lambda/D\cos\theta] - [\varepsilon^* \tan\theta] \quad (2)$$

where  $\varepsilon^*$  is the dimensionless strain value.

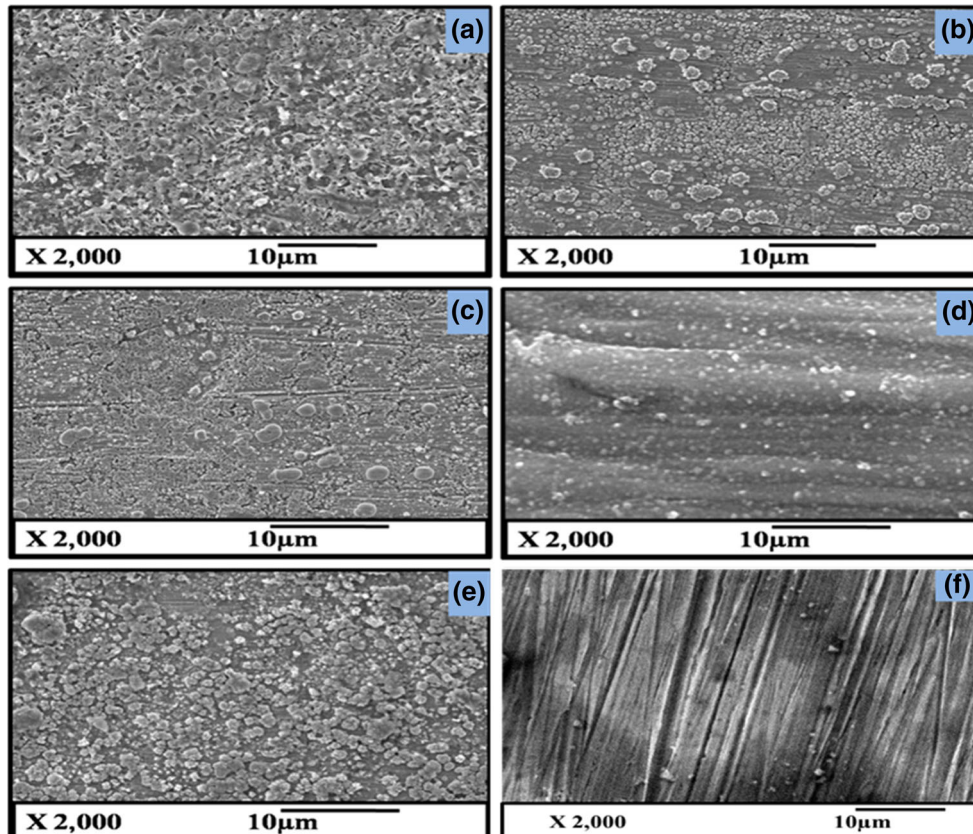
Table 2 shows the variation of induced stress and lattice strains in the electrodeposited Ni–Zn alloy coatings for the prominent (101) peak. The variation in the values of stress and strain can be seen as an effect of saccharin addition. Saccharin with  $1.6 \text{ g L}^{-1}$  shows low values of stress and strain

due to the formation of smooth and compact morphology as confirmed from the SEM images. As the saccharin content is increased up to  $1.8 \text{ g L}^{-1}$ , the induced stress is increased due to the formation of a non-compact cracked morphology as evident from the SEM images.

### Microstructure of Ni–Zn alloy coatings

In the absence of saccharin, a rough, random and non-compact, matt and dark network of the Ni–Zn alloy is formed. The spherical aggregated interlinked particles in the grain size between 290 and 320 nm are shown in Fig. 3a. Here, many individual grain boundaries are visible which accelerate the corrosion process. With the addition of  $0.7 \text{ g L}^{-1}$  saccharin addition, clusters of spherical grains with non-uniform sizes are observed as shown in Fig. 3b in the range of 170–230 nm. From the image, it is seen that grain numbers are reduced and many grains have merged with each other. This may be due to the unavailability of sufficient saccharin molecules to favorably reduce Zn ions in the Ni–Zn alloy film. When  $1.4 \text{ g L}^{-1}$  saccharin was added, it favored Zn deposition in the Ni–Zn alloy to form a uniform film as shown in Fig. 3c. Figure 3d indicates the case of  $1.6 \text{ g L}^{-1}$  saccharin addition which resulted into a compact, uniform, and smooth deposition of a Zn-rich Ni–Zn film having grains of 80–90 nm size. As seen

**Fig. 3** The SEM images of Ni–Zn alloy coating deposited from saccharin addition as **a**  $0 \text{ g L}^{-1}$ , **b**  $0.7 \text{ g L}^{-1}$ , **c**  $1.4 \text{ g L}^{-1}$ , **d**  $1.6 \text{ g L}^{-1}$ , **e**  $1.8 \text{ g L}^{-1}$  in the bath, and **f** the SEM image of the naked steel substrate



from the image, it is seen that the number of grain boundaries is reduced as most of the grains have merged with each other producing a uniform and compact deposit. This may be due to the synergistic effect of saccharin to reduce Zn ions to produce films with low stress. Saccharin addition induces grain refinement effect along with a restriction to grain boundary sliding [3]. The change in the Zn content in the Ni–Zn alloy with varying saccharin content is reflected as the change in the morphology due to change in the composition of the alloy compound as confirmed from Table 2. Generally, for coatings, the compact microstructure is desirable. The presence of a non-compact and cracked microstructure initiates the corrosion process at the extent of grain boundaries. So if the grain boundaries are less and the microstructure is compact, the corrosion process is prevented. Figure 3e shows uneven and

non-uniform aggregated spherical grains with the size varying from 120 to 180 nm as a result of the excess addition of saccharin. This effect may be attributed due to the variation in the composition of the Helmholtz layer and induction of carbon and sulfur impurities in the deposits due to excess saccharin addition [3]. Figure 3f represents the FESEM image of the naked steel substrate for reference comparison between the coated and uncoated steel surface.

### Surface topography of Ni–Zn alloy deposit

The three-dimensional (3D) surface topography of Ni–Zn alloy coatings was studied using the AFM technique. The AFM 3D images in Fig. 4a–e are of the Ni–Zn alloy coatings produced from 0, 0.7, 1.4, 1.6, and 1.8 g L<sup>-1</sup> saccharin-containing

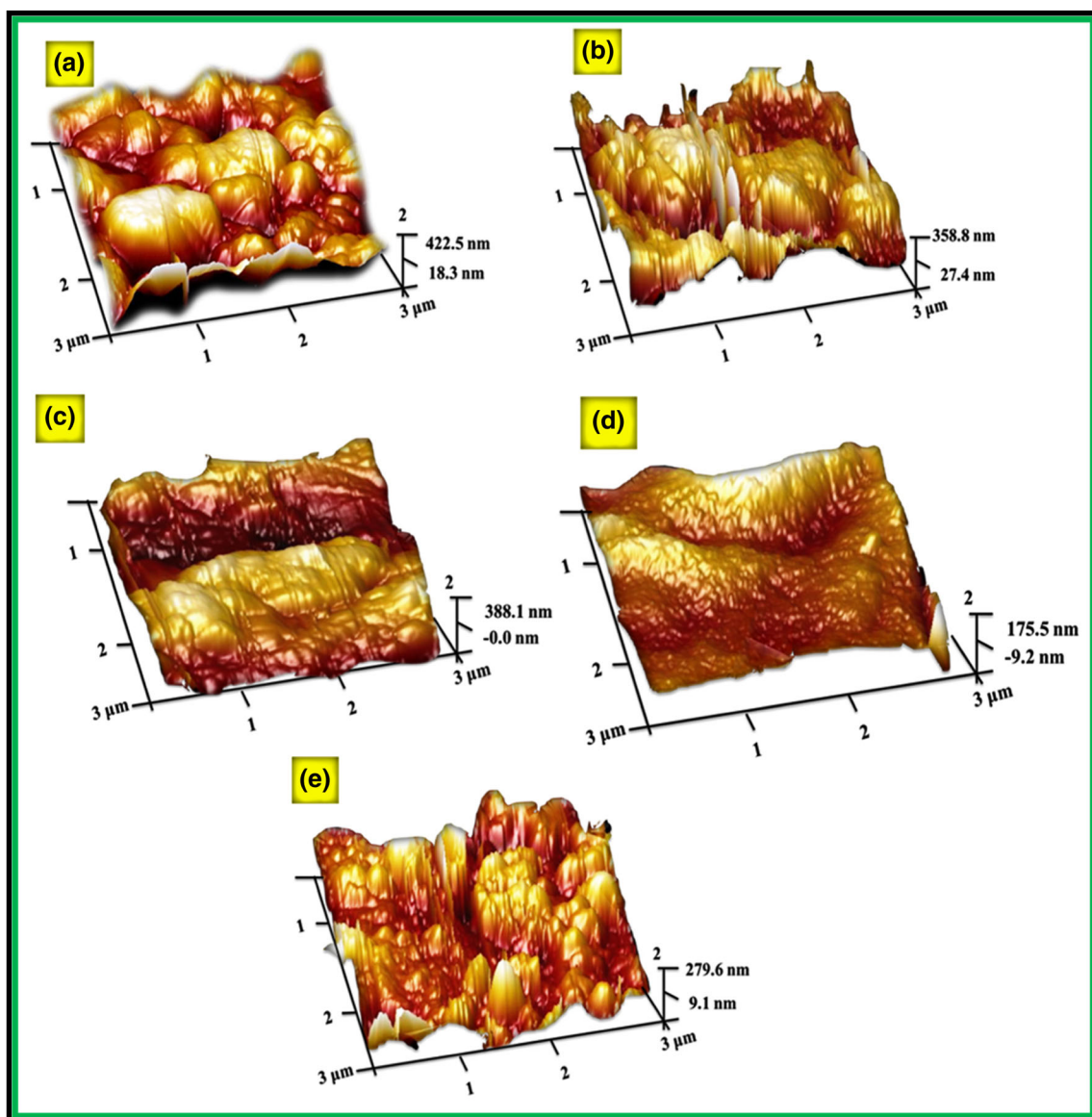


**Fig. 4** The three-dimensional (3D) AFM images of Ni–Zn alloy coatings deposited from bath containing saccharin addition as **a** 0 g L<sup>-1</sup>, **b** 0.7 g L<sup>-1</sup>, **c** 1.4 g L<sup>-1</sup>, **d** 1.6 g L<sup>-1</sup>, and **e** 1.8 g L<sup>-1</sup>

baths, respectively. Table 3 shows the values of surface roughness, grain size, and grain height for various saccharin contents in the deposition bath. The significant reductions in the grain size from 320 to 94 nm and roughness value from 104 to 30 nm result from increased saccharin addition from 0 to 1.6 g L<sup>-1</sup>. There is a considerable reduction in the grain height from 422 to 175 nm. From the AFM study, it is seen that for 1.6 g L<sup>-1</sup> saccharin addition, nanograins of uniform size and shapes are formed. The growth of the alloy coatings occurs in two stages such as nucleation and grain growth. As the deposition process is initiated, many new active nucleation sites are formed. Saccharin addition in the deposition bath induces a chemical barrier to adions and adatoms on the coated surface preventing them from reaching active nucleation sites and thereby restricting the grain growth process [3]. This is the major reason for reducing the grain size and grain height after saccharin addition. The number of the grain boundary is reduced producing a uniform and compact deposit with reduced roughness value. Beyond 1.6 g L<sup>-1</sup> saccharin addition, the values of grain height, grain size, and roughness as seen in Table 3 increases due to the variation in the composition of the Helmholtz layer mentioned earlier in the SEM study.

### Contact angle of Ni–Zn alloy coatings

Controlling the surface wettability of solid surfaces is important in many situations. If the wettability is high, the contact angle ( $\theta < 90^\circ$ ) is small and the surface is hydrophilic, and if the wettability is low, the contact angle ( $\theta > 90^\circ$ ) is large and the surface is hydrophobic. The surface tension of the liquid and the interfacial tension between solid and liquid decides the contact angle [18]. The contact angle measurement was carried out to understand the affinity of electrolyte towards the Ni–Zn coating. For Ni–Zn coating with 0, 0.7, 1.4, 1.6, and 1.8 g L<sup>-1</sup>, the contact angles were found to be 21°, 27°, 34°, 65°, and 46°, respectively. The lowest contact angle of 21° implies a favorable interaction between Ni–Zn coating and water, which may be responsible for the higher corrosion rate. For deposits with 0.7 and 1.4 g L<sup>-1</sup> addition of saccharin, there

is no appreciable increase in contact angle indicating low corrosion-resistant deposits. But for Ni–Zn deposition with 1.6 g L<sup>-1</sup> saccharin addition, the contact angle remarkably increased to 65° as shown in Fig. 5 which favors good corrosion resistance of the Ni–Zn coating. As the contact angle increases with the addition of saccharin, the corrosion resistance of the coating also increases because there is minimum scope for the liquid medium to spread over the coated surface. For 1.8 g L<sup>-1</sup> addition of saccharin, the contact angle decreased to 46° thereby signifying unsuitability to use as a corrosion-resistant material. Table 3 shows the variation in the contact angle with varied saccharin content addition. This reduction in the contact angle value is due to the formation of a non-compact morphology which allows the liquid medium to spread easily over the coated surface. Thus, it is clear that the electrodeposited Ni–Zn alloy coating without and with saccharin additions is hydrophilic in nature.

### Electrochemical impedance study of Ni–Zn alloy coatings

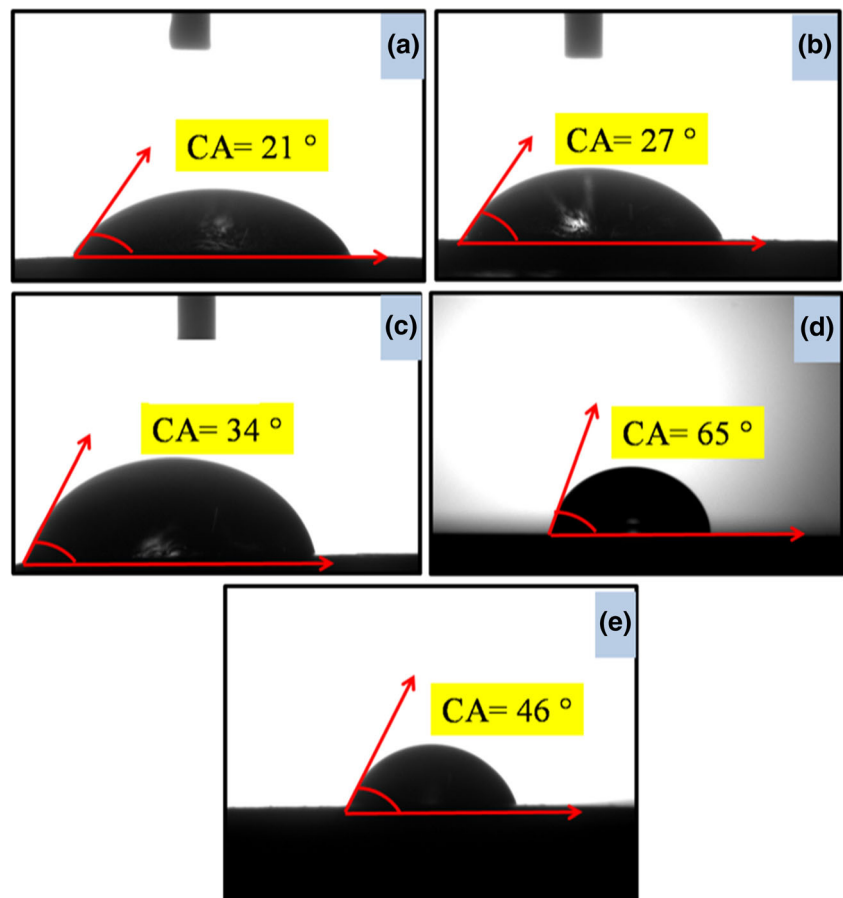
EIS is an important technique to determine the corrosion of coatings. Figure 6 (a–e) shows the Nyquist plots of the Ni–Zn alloy coating in 5% NaCl solution with an applied bias of 10 mV, where  $Z'(\omega)$  and  $Z''(\omega)$  are the real and imaginary parts of the measured impedance, respectively, and  $\omega$  is the angular frequency. The higher impedance value and the larger diameter of the (incomplete) semicircle in the spectra of the Ni–Zn alloy show its higher corrosion resistance, which can be related to the variation in the film (coating) capacitance. As the reactance of the film is given by, i.e.,  $X_c = 1/2\pi f c$ , the diameter of the semicircle increases, and the imaginary part of  $X_c$  on the y-axis also increases. This means that at fixed frequency, the capacitance of the film decreases for a larger value of  $X_c$ . In our case, it is better to have a large value of  $X_c$  (capacitive impedance) because it contributes to high corrosion resistance [19].

Two semicircles appear in the plots indicating two relaxation processes in the lower and higher frequency range. The semicircle in the lower frequency range arises as a result of the activation process while that in the high-frequency region relates to the oxide layer [12]. The higher impedance value in the lower and higher frequency ranges indicates the higher oxidation and corrosion resistance. Figure 5a–e shows the Nyquist plots of the Ni–Zn alloy with 0, 0.7, 1.4, 1.6, and 1.8 g L<sup>-1</sup> saccharin additions with impedance values of 640, 695, 850, 874, and 815  $\Omega \text{ cm}^{-2}$ , respectively. The increased impedance value from 640 to 874  $\Omega \text{ cm}^{-2}$  results from an effect of increased saccharin addition to 1.6 g L<sup>-1</sup> producing a smooth and compact morphology. As explained in the SEM study, the presence of a non-compact and cracked microstructure initiates the corrosion process at the extent of grain boundaries because many active sites are generated at grain boundaries which are responsible for the initiating corrosion

**Table 3** The effect of saccharin content on the surface properties, contact angle, and impedance value of Ni–Zn alloy coatings

Saccharin content (g L <sup>-1</sup> ) in deposition bath	Surface roughness (nm)	Grain size (nm)	Grain height (nm)	Contact angle (°)
0	104	320	422	21
0.7	99.7	190	388	27
1.4	75.5	230	358.8	34
1.6	30	94.34	175	65
1.8	48.7	120	279	46

**Fig. 5** Contact angle measurement with varied saccharin content in the bath



process. Hence, at  $1.6 \text{ g L}^{-1}$  saccharin addition, a very compact microstructure with fewer grain boundaries is formed which will provide the lowest possible scope to initiate corrosion. Saccharin with  $1.6 \text{ g L}^{-1}$  addition resulted in increased Zn composition in Ni–Zn alloy coating as confirmed from the AAS and XRD studies. Zn provides more cathodic protection than Ni and so the significantly increased impedance value from  $695$  to  $850 \text{ } \Omega \text{ cm}^{-2}$  and further on is due to the Zn-rich

HCP phase structure of Zn in the Ni–Zn alloy coating. The additional saccharin content in the bath up to  $1.8 \text{ g L}^{-1}$  resulted in the reduction in the impedance value to  $815 \text{ } \Omega \text{ cm}^{-2}$  as seen in Fig. 5e due to the formation of a non-compact microstructure with many numbers of grain boundaries. The well-fitted circuit included in Fig. 5 indicates the increase in the equivalent series resistance (Table 4) with increasing saccharin concentration up to  $1.6 \text{ g L}^{-1}$ . Table 4 shows the variation

**Fig. 6** The Nyquist plots of the Ni–Zn alloy coating in 5% NaCl solution with saccharin addition in the bath as a  $0 \text{ g L}^{-1}$ , b  $0.7 \text{ g L}^{-1}$ , c  $1.4 \text{ g L}^{-1}$ , d  $1.6 \text{ g L}^{-1}$ , and e  $1.8 \text{ g L}^{-1}$

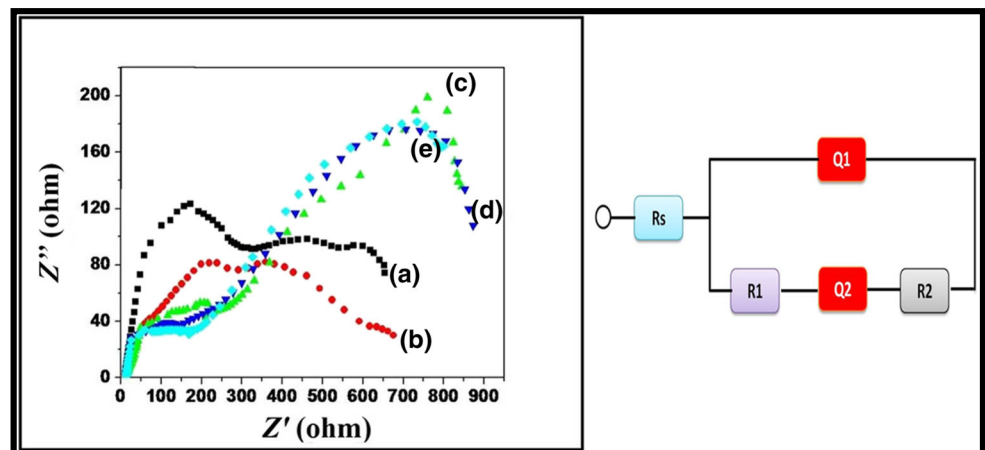




**Table 4** The effect of saccharin content on the time for the appearance of red rust on the fasteners with Ni–Zn alloy coatings

Saccharin content (g L <sup>-1</sup> )	Time for complete oxidation of the fastener in 5% NaCl solution (h)	Impedance value (Ω cm <sup>-2</sup> )	Equivalent series resistance (Rs)
0	1320	640	0.42
0.7	1450	695	0.63
1.4	1640	850	0.68
1.6	1700	874	0.75
1.8	1610	815	0.71

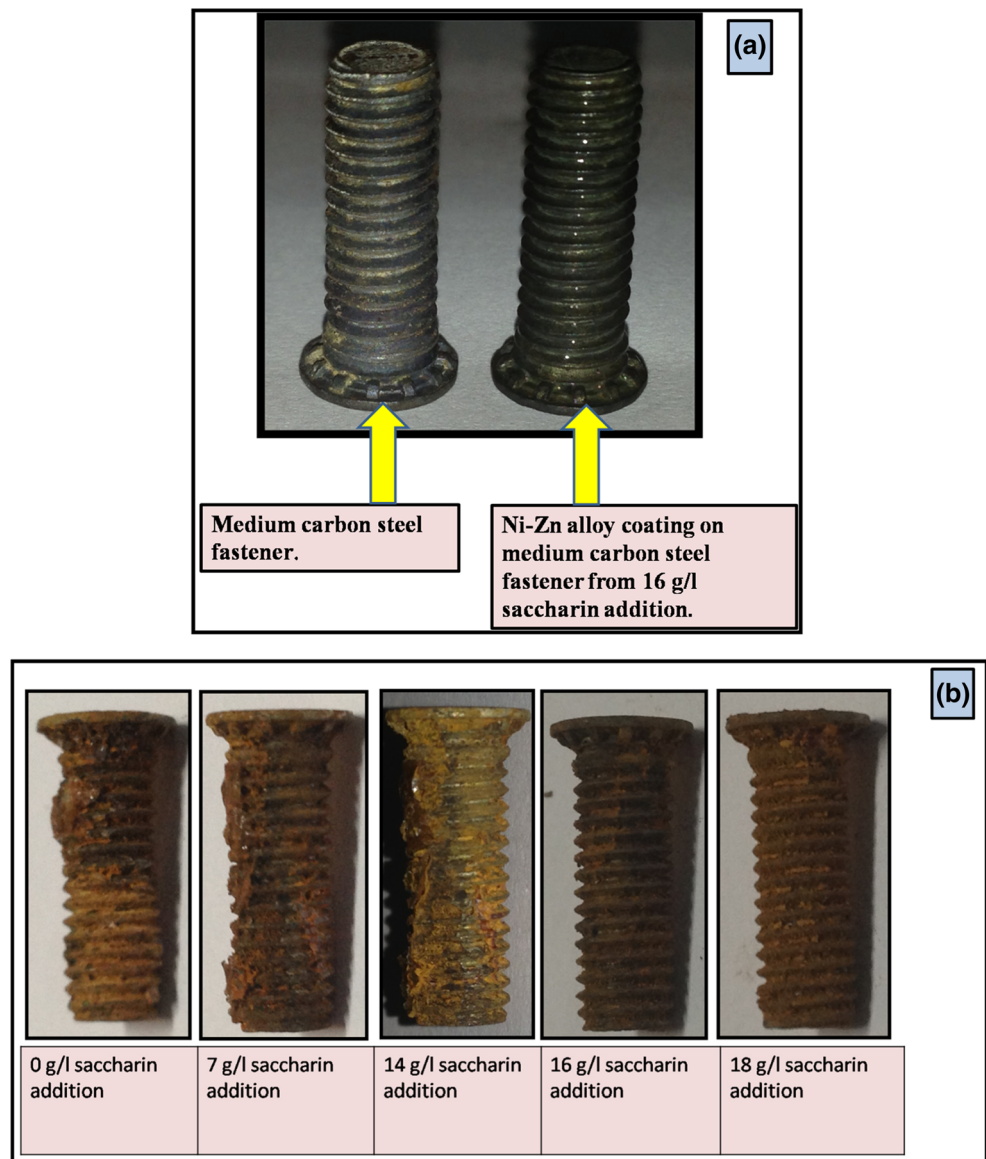
in the impedance values with varied saccharin content addition in the bath. The reduced impedance value is attributed due to the non-compact microstructure with many grain

boundaries which increases the interaction between NaCl solution and coated surface.

**Salt immersion test (5% NaCl solution test)**

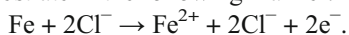
This study aims to induce the corrosive environment in order to determine the corrosion resistance of coating in terms of time (h). The Ni–Zn alloy coated on medium carbon steel fasteners was kept immersed in 5% NaCl solution at room temperature, and the time for the appearance of the red rust on the coated surface was observed. Figure 6 (a) shows photographs of the coatings without and with electrodeposited Ni–Zn alloy on medium carbon steel fasteners. Figure 7b shows a photograph of rusted Ni–Zn alloy-coated fasteners with 0, 0.7, 1.4, 1.6, and 1.8 g L<sup>-1</sup> saccharin addition in the bath immersed in 5% NaCl for 1700 h. Table 4 shows the time

**Fig. 7 a** The photograph of electrodeposited Ni–Zn alloy coating on medium carbon steel fasteners. **b** Photograph of the rusted Ni–Zn alloy-coated fasteners with 0, 0.7, 1.4, 1.6, and 1.8 g L<sup>-1</sup> saccharin addition, kept immersed in 5% NaCl solution for 1700 h

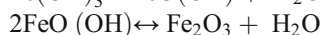


for the complete oxidation of the Ni–Zn alloy-coated fasteners. From Table 4, it is clear that Ni–Zn alloy-coated fasteners with  $1.6 \text{ g L}^{-1}$  saccharin addition has maximum time for complete oxidation indicating maximum resistance to corrosion as compared to other fasteners. The results obtained from this study match with the EIS study confirming that the Ni–Zn alloy coating from  $1.6 \text{ g L}^{-1}$  saccharin addition in the bath has maximum corrosion resistance. The corrosion behavior of the Ni–Zn alloy carried out in 5% NaCl solution leads to water reduction which leads to the formation pits of  $\text{Ni(OH)}_2$  and  $\text{Zn(OH)}_2$ . The by-products like  $\text{NiCl}_2$  and  $\text{ZnCl}_2$  may be formed. The  $\text{Na}^+$  and  $\text{Cl}^-$  ions go into these pits. The regions of  $\text{Na}^+$  diffusion are cathodic sites while the regions of  $\text{Cl}^-$  diffusion are anodic sites. Thus, sodium is aggregated by migration and diffusion. With time, these  $\text{Na}^+$  ions penetrate into the carbon steel substrate near the outside boundary of the pit while  $\text{Cl}^-$  ion penetrates inside pits of the carbon steel.

The penetrated  $\text{Cl}^-$  ions react with Fe of the carbon steel substrate in the following manner:



The oxidized  $\text{Fe}^{2+}$  ion reacts with  $\text{H}_2\text{O}$  to form  $\text{Fe(OH)}_2$ . This may further react with  $\text{H}_2\text{O}$  to form  $\text{Fe(OH)}_3$ .



Thus, red rust of  $\text{Fe}_2\text{O}_3$  is formed. The other corrosion products such as  $\text{ZnO}$ ,  $\text{Zn}_5(\text{OH})_8\text{Cl}_2 \cdot \text{H}_2\text{O}$ ,  $\text{Na}_2\text{Zn}_3(\text{CO}_3)_4(\text{H}_2\text{O})_3$ , and  $\text{Zn(OH)}_2$  may also be formed [20].

### Friction coefficient and wear resistance of Ni–Zn alloy coatings

Figure 8 (a, b) shows the friction coefficient value ( $\mu$ ) of the Ni–Zn alloy coatings at various saccharin content additions.

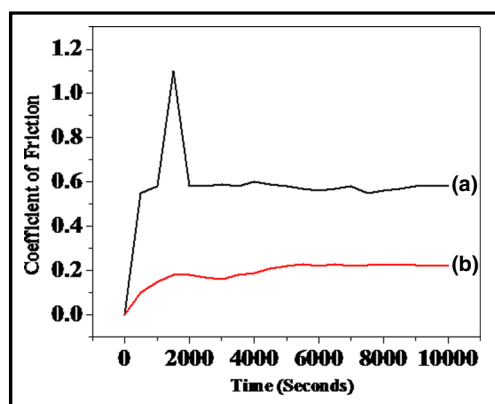


**Fig. 8** *a* The plot of friction coefficient value ( $\mu$ ) of the Ni–Zn alloy coating without saccharin addition ( $0 \text{ g L}^{-1}$ ). *b* The plot of the friction coefficient value of the Ni–Zn alloy coating with  $1.6 \text{ g L}^{-1}$  saccharin addition

The plot in Fig. 8 (a) shows the value of the friction coefficient ( $\mu$ ) against the sliding time. Initially, the  $\mu$  value starts from 0 and reaches a value of about 0.55. After a time lapse of 1500 s, the  $\mu$  value shoots to 1.1 and then attains a stable constant average value of 0.58. Fluctuations are observed in the graph due to the wear of the Ni–Zn alloy-coated surface during sliding and its effect of acting as a third body resistance between the pin and the coated Ni–Zn alloy surface. The friction coefficient value ( $\mu$ ) 0.58 is mainly attributed due to the mixed phase structure of the Ni–Zn alloy and the non-compact morphology. Figure 8 (b) represents the friction coefficient value ( $\mu$ ) of the Ni–Zn alloy with  $1.6 \text{ g L}^{-1}$  saccharin addition. The value of  $\mu$  in this case reduces up to 0.225. This effect of reduction in the  $\mu$  value is mainly due to saccharin  $1.6 \text{ g L}^{-1}$  addition which produces a smooth and compact morphology with a hexagonal rich phase structure of Zn in the Ni–Zn alloy. It may be stated that the friction coefficient value ( $\mu$ ) can be reduced using saccharin as an additive agent. Wang et al. [4] reported a reduced friction coefficient value up to 0.25 of the electrodeposited Ni–Co alloy with increased Co content up to 80%. Lokhande et al. [21] reported a friction coefficient value of deposited Ni–Co alloy as 0.69 using saccharin as an additive which is considered a moderate value.

Figure 9 (a) shows the wear with a time of Ni–Zn alloy coating without saccharin addition. The wear initiates from  $0 \mu\text{m}$  as seen in the figure and attains a value of  $490 \mu\text{m}$  wear within a time span of 1000 s. After 1000 s, the wear decreases and attains a stable average constant value of  $100 \mu\text{m}$  for a time lapse of 2500 s. After 2500 s, the wear curve goes on reducing and attains a negative value with a smooth curve with no fluctuations which indicates that there is total wear-out of the Ni–Zn alloy coating and the sliding action occurs between the ball and the medium carbon steel substrate. Hence from the figure, it is quite clear that the Ni–Zn alloy coating without saccharin addition has wear of  $100 \mu\text{m}$  for a time span of 2500 s with an applied load of 6 N. In other words, it can be stated that the Ni–Zn alloy coating lasts

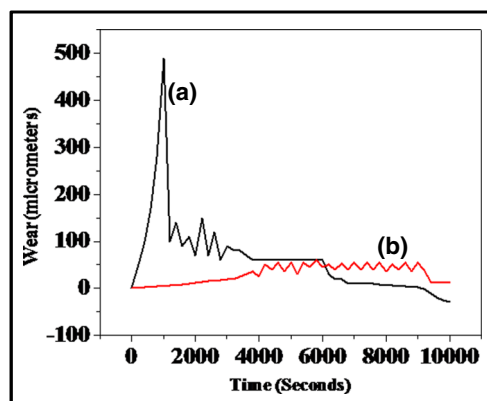


**Fig. 9** *a* The plot of wear resistance of the Ni–Zn alloy coating without saccharin addition ( $0 \text{ g L}^{-1}$ ). *b* The plot of wear resistance of the Ni–Zn alloy coating with  $1.6 \text{ g L}^{-1}$  saccharin addition

throughout the wear test for 2500 s with an applied load of about 6 N.

Figure 9 (b) shows the plot of wear with a time of Ni–Zn alloy coatings with  $1.6 \text{ g L}^{-1}$  saccharin addition. The wear gradually increases up to the value of  $45 \text{ }\mu\text{m}$  within the time span of 3800 s. This wear value remains constant up to the time of 9000 s. Beyond the time span of 9000 s, the wear graph becomes smooth with no fluctuations indicating the total wear-out of the Ni–Zn alloy coating as mentioned in the earlier result. Thus, it is clear that Ni–Zn alloy coatings with  $1.6 \text{ g L}^{-1}$  saccharin addition are more wear resistant than the alloy with no saccharin addition as it has wear of about  $45 \text{ }\mu\text{m}$  and lasts throughout the wear test up to 9000 s. The increased wear resistance of the Ni–Zn alloy coating with  $1.6 \text{ g L}^{-1}$  saccharin addition is due to the smooth, compact, and adherent deposition of the alloy coatings.

## Conclusions

The electrodeposition of Ni–Zn alloy coatings from a sulfate bath using a varied amount of saccharin (0 to  $1.8 \text{ g L}^{-1}$ ) as an additive agent has been carried out. The deposition of the Ni–Zn alloy coating is of the anomalous type where less noble metal Zn is preferentially deposited over nickel. The alloy composition of Ni–Zn varied between 64:36 and 22:78 at.% depending on saccharin content addition in the deposition bath proving that the saccharin addition in the deposition bath favors the deposition of Zn over Ni. Ni–Zn alloy coatings are hydrophilic in nature. Saccharin with  $1.6 \text{ g L}^{-1}$  addition in the deposition bath produces low stressed deposits with a smooth, fine-grained, and compact morphology. Desirable effects such as inhabitation of grain growth, grain refinement, reduced grain boundary number, improved corrosion and wear resistance, reduced surface roughness, and reduced residual stress and friction coefficient value are obtained for Ni–Zn alloy coating with  $1.6 \text{ g L}^{-1}$  saccharin addition at Ni 25 at.% and Zn 75 at.%.

**Acknowledgements** This work was supported by the Human Resources Development program (No. 20124010203180) of the Korea Institute of Energy Technology Evaluation and Planning (KETEP) Grant funded by the Korean government Ministry of Trade, Industry, and Energy and supported by the Basic Science Research Program through the National Research Foundation of Korea (NRF) funded by the Ministry of Science, ICT, and Future Planning (NRF-2015R1A2A2A01006856).

## References

- Heinrich U, Peters L, Ernst H, Rittinghausen S, Dasenbrock C, König H (1989) Investigation of the carcinogenic effects of various cadmium compounds after inhalation in hamsters and mice. *Exp Pathol* 37:253–258
- Ganesan P, Kumaraguru SP, Popov BN (2006) Development of Zn–Ni–Cd coatings by pulse electrodeposition process. *Surf Coat Technol* 201:3658–3669
- Mosavat SH, Bahrololoom ME, Shariat MH (2011) Electrodeposition of nanocrystalline Zn–Ni alloy from alkaline glycinate bath containing saccharin as additive. *Appl Surf Sci* 257:8311–8316
- Wang L, Gao Y, Xue Q, Liu H, Xu T (2005) Microstructure and tribological properties of electrodeposited Ni–Co alloy deposits. *Appl Surf Sci* 242:326–332
- Li Y, Jiang H, Wang D, Ge H (2008) Effects of saccharin and cobalt concentration in electrolytic solution on microhardness of nanocrystalline Ni–Co alloys. *Surf Coat Technol* 202:4952–4956
- Walter RJ (1986) Tensile properties of electrodeposited nickel-cobalt. *Plat Surf Finish* 73:48
- Rao VR, Bangera KV, Hegde AC (2013) Magnetically induced electrodeposition of Zn–Ni alloy coatings and their corrosion behaviors. *J Magn Magn Mater* 345:48–54
- Byk TV, Gaevsкая TV, Tsybul'skaya LS (2008) Effect of electrodeposition conditions on the composition, microstructure, and corrosion resistance of Zn–Ni alloy coatings. *Surf Coat Technol* 202:5817–5823
- Hammami O, Dhouibi L, Triki E (2009) Influence of Zn–Ni alloy electrodeposition techniques on the coating corrosion behavior in chloride solution. *Surf Coat Technol* 203:2863–2870
- Sorkhabi HA, Hagrah A, Ahmadi NP, Manzoori J (2001) Zinc–nickel alloy coatings electrodeposited from a chloride bath using direct and pulse current. *Surf Coat Technol* 140:278–283
- Qiao X, Li H, Zhao W, Li D (2013) Effects of deposition temperature on electrodeposition of zinc–nickel alloy coatings. *Electrochim Acta* 89:771–777
- Hegde AC, Venkatakrishna K, Eliaz N (2010) Electrodeposition of Zn–Ni, Zn–Fe and Zn–Ni–Fe alloys. *Surf Coat Technol* 205:2031–2041
- Eliaz N, Venkatakrishna K, Hegde AC (2010) Electroplating and characterization of Zn–Ni, Zn–Co and Zn–Ni–Co alloys. *Surf Coat Technol* 205:1969–1978
- Brenner A (1963) *Electrodeposition of alloys*. Academic Press, New York
- Altamirano-Gracia L, Vazquez-Arenas J, Pritzker M, Luna-Sanchez R, Cabrera-Sierra R (2015) Effects of saccharin and anions ( $\text{SO}_4^{2-}$ ,  $\text{Cl}^-$ ) on the electrodeposition of Co–Ni alloys. *J Solid State Electrochem* 19:423–433
- Miranda FJF, Barcia OE, Diaz SL, Mattos OR, Wiat R (1996) Electrodeposition of Zn–Ni alloys in sulfate electrolytes. *Electrochim Acta* 41:1041–1049
- Barceló G, Sarret M, Müller C, Pregonas J (1998) Corrosion resistance and mechanical properties of zinc electrocoatings. *Electrochim Acta* 43:13–20
- Shinde NM, Lokhande AC, Lokhande CD (2014) A green synthesis method for large area silver thin film containing nanoparticles. *J Photochem Photobiol* 136:19–25
- Cantini NJ, Mitton DB, Eliaz N, Leisk G, Wallace SL, Bellucci F, Thompson GE, Latanision RM (2000) In situ underfilm corrosion rate measurements by magnetic and electrochemical techniques. *Electrochem. Solid State Lett* 3:275–278
- Sajjadnejad M, Mozafari A, Omidvar H, Javanbakht M (2014) Preparation and corrosion resistance of pulse electrodeposited Zn and Zn–SiC nanocomposite coatings. *Appl Surf Sci* 300:1–7
- Lokhande AC, Bagi JS (2014) Studies on enhancement of surface mechanical properties of electrodeposited Ni–Co alloy coatings due to saccharin additive. *Surf Coat Technol* 258:225–231